

Published in final edited form as:

Cell Rep. 2013 September 12; 4(5): . doi:10.1016/j.celrep.2013.08.002.

NLRP3 inflammasome blockade inhibits VEGF-A induced age-related macular degeneration

Alexander Georg Marneros

Cutaneous Biology Research Center, Massachusetts General Hospital, and Department of Dermatology, Harvard Medical School, Charlestown, MA 02129, USA

Summary

The NLRP3 inflammasome is activated in age-related macular degeneration (AMD), but it remains unknown whether its activation contributes to AMD pathologies. VEGF-A is increased in neovascular (“wet”) AMD, but it is not known whether it plays a role in inflammasome activation, whether an increase of VEGF-A by itself is sufficient to cause neovascular AMD, and whether it can contribute to nonexudative (“dry”) AMD that often co-occurs with the neovascular form. Here it is shown that an increase in VEGF-A results in NLRP3 inflammasome activation and is sufficient to cause both forms of AMD pathologies. Targeting NLRP3 or the inflammasome effector cytokine IL-1 β inhibits but does not prevent VEGF-A-induced AMD pathologies, while targeting IL-18 promotes AMD. Thus, increased VEGF-A provides a unifying pathomechanism for both forms of AMD; combining therapeutic inhibition of both VEGF-A and IL-1 β or the NLRP3 inflammasome is therefore likely to suppress both forms of AMD.

Introduction

Age-related macular degeneration (AMD) is the most common cause of irreversible blindness in the elderly (Friedman et al., 2004; van Leeuwen et al., 2003). AMD manifests with the cardinal features of progressive atrophic degeneration of the retinal pigment epithelium (RPE) with sub-RPE deposits that affect metabolic exchanges between the RPE and choroidal vessels in nonexudative (“dry”) AMD, or with choroidal neovascularization (CNV) in neovascular (“wet”) AMD (Bird et al., 1995; Kliffen et al., 1997). Importantly, patients with nonexudative AMD can progress to develop neovascular AMD, and both forms of AMD can occur simultaneously, suggesting a common pathomechanism that is currently unknown, in part due to the lack of a mouse model with features of both forms of AMD (Sunnus et al., 1999).

Increased VEGF-A levels have been observed in neovascular AMD, but it remains to be shown whether an increase in VEGF-A alone is sufficient to cause neovascular AMD and through which pathomechanisms it may promote the disease process (Funk et al., 2009; Klettner and Roider, 2009). Increased hypoxia and oxidative damage to the RPE have been regarded as critical factors in AMD pathogenesis, which induce VEGF-A expression in the

© 2013 The Authors. Published by Elsevier Inc. All rights reserved.

Correspondence: Alexander G. Marneros, M.D., Ph.D., CNY-149, Rm 3.216, CBRC, MGH East, 13th Street, Charlestown, MA, 02129, Tel.: 6176437170; Fax.: 6177264453, amarneros@partners.org.

No conflict of interest is reported.

Publisher's Disclaimer: This is a PDF file of an unedited manuscript that has been accepted for publication. As a service to our customers we are providing this early version of the manuscript. The manuscript will undergo copyediting, typesetting, and review of the resulting proof before it is published in its final citable form. Please note that during the production process errors may be discovered which could affect the content, and all legal disclaimers that apply to the journal pertain.

RPE (Funk et al., 2009; Klettner and Roeder, 2009). Consistent with the observed increased VEGF-A levels in neovascular AMD, anti-VEGF-A treatments have shown significant clinical benefit in patients with neovascular AMD (Martin et al., 2011). In contrast, nonexudative AMD is more common than neovascular AMD and causes loss of vision in millions of individuals, but no established treatments exist for nonexudative AMD. Thus, identifying a common pathogenetic step for both forms of AMD would provide the opportunity for a targeted broad therapeutic approach for neovascular and nonexudative AMD.

Genetic association data have provided evidence for linkage of both forms of advanced AMD with the VEGF-A gene locus (Fritsche et al., 2013) (Yu et al., 2011), suggesting that increased VEGF-A levels may promote not only neovascular AMD, but also nonexudative AMD. Thus, both forms of AMD may arise as distinct manifestations of a common underlying process of VEGF-A dysregulation.

Recently, NLRP3 inflammasome activation has been reported in both nonexudative and neovascular AMD, but it is not known whether VEGF-A promotes its activation (Kaneko et al., 2011; Tarallo et al., 2012; Tseng et al., 2013). Activation of the NLRP3 inflammasome results in autocatalytic cleavage of caspase-1 precursor (with the generation of the active p10 and p20 subunits), which leads to proteolytic activation of the potent pro-inflammatory cytokines IL-1 and IL-18 (Latz et al., 2013). Importantly, inflammasome activation has been suggested to influence various metabolic and aging diseases, including atherosclerosis, diabetes, gout or obesity (Wen et al., 2012). However, it is not known whether NLRP3 inflammasome activation has a pathogenic role in the development of AMD, due to the lack of a mouse model that manifests chorioretinal pathologies as seen in both forms of AMD with progressive age, in which the role of the inflammasome could be tested. Recent studies have proposed either an inhibitory or a promoting role of the NLRP3 inflammasome for AMD (Doyle et al., 2012; Tarallo et al., 2012). Inhibition of the NLRP3 inflammasome prevented RPE degeneration, induced by DICER1 loss or *Alu* RNA exposure, while it increased neovascular lesions in an acute laser wound-healing model (Doyle et al., 2012; Tarallo et al., 2012). However, these studies were limited by the use of experimental models that do not reflect the age-dependent progressive pathologies seen in AMD, such as the acute laser injury-model in which neovascularization occurs in the setting of healthy RPE cells, which is in fact an acute wound healing model and only a very limited model for neovascular AMD (He and Marneros, 2013). Thus, the role of the NLRP3 inflammasome in such an acute wound healing model is likely to differ from its role in human AMD or in a mouse model that develops cardinal features of AMD in a progressive age-dependent manner accompanied by degenerative RPE changes.

Here, mice with increased VEGF-A levels are shown to develop age-dependent progressive cardinal features of both nonexudative and neovascular AMD, in which NLRP3 inflammasome activation occurs as seen in human AMD. Targeting NLRP3 or the inflammasome effector cytokine IL-1 reduces VEGF-A induced chorioretinal pathologies in these mice, such as RPE barrier breakdown and CNV lesions, while IL-18 deficiency promotes CNV lesions. The data provide a unifying pathomechanism for both forms of AMD and show that what has been considered as a multifactorial pathogenesis can be triggered by an increase of a single growth factor, VEGF-A, which induces NLRP3 inflammasome activation to promote AMD-like pathologies.

Results

An age-dependent RPE barrier breakdown in mice with increased VEGF-A levels

To determine whether an increase in VEGF-A by itself is sufficient to cause eye pathologies as seen in AMD, mutant mice were analyzed that have increased VEGF-A protein levels. The increase of VEGF-A levels occurs in adult heterozygote VEGF-A^{lacZKI/WT} mice (hereafter described as VEGF-A^{hyper} mice) as a consequence of the insertion of an IRES-NLS-lacZ-SV40pA sequence into the 3'-UTR region of the VEGF-A gene locus at +202 bp 3' to the stop codon (Cervi et al., 2007; Miquerol et al., 1999), which removes miRNA binding sites in the 3' UTR that would inhibit VEGF-A mRNA translation (Jafarifar et al., 2011). Adult transgenic mice that express lacZ driven by a promoter that is active in RPE cells (Dct-lacZ-SV40pA mice) (Wilkie et al., 2002) showed no eye abnormalities, suggesting that changes observed in the eyes of VEGF-A^{hyper} mice are due to increased VEGF-A levels and not due to the insertion of the lacZ sequence and β -galactosidase expression in RPE cells. In additional control experiments, mice were examined in which the IRES-NLS-lacZ-SV40pA sequence was inserted immediately after the VEGF-A stop codon, resulting in a hypomorphic VEGF-A allele (VEGF-A^{hypo} mice) while maintaining β -galactosidase expression from the endogenous VEGF-A locus (Damert et al., 2002). These VEGF-A^{hypo} mice showed β -galactosidase expression in ocular tissues like VEGF-A^{hyper} mice, but without ocular pathologies, further demonstrating that the observed eye changes in VEGF-A^{hyper} mice are due to the increased VEGF-A levels (Figures 1J-K).

In these VEGF-A^{hyper} mice nuclear β -galactosidase expression (due to the nuclear localization signal between the IRES sequence and the lacZ) reflects accurately VEGF-A expression at single-cell resolution (Figures 1A, S1A-B). The use of an IRES sequence allows independent translation of both VEGF-A and the lacZ-reporter from the same bicistronic mRNA produced by the targeted allele. Choroid/RPE tissues as well as retinas from adult VEGF-A^{hyper} mice showed significantly increased VEGF-A protein levels compared to control littermate mice, albeit retinas having lower VEGF-A levels (Figure 1B). Consistent with this observation, staining for β -galactosidase showed that RPE cells are the main cell type in the choroid and retina to express VEGF-A, and that strong VEGF-A expression in the RPE is maintained at all ages (up to 24 months old mice were studied) (Figure 1A). Similarly, VEGF-A serum levels were increased in VEGF-A^{hyper} mice and this increase was maintained with progressive age (Figure 1B). A cell line derived from human RPE cells, ARPE-19 cells, and freshly isolated primary mouse RPE cells express the VEGF-A receptors Flt1 and Flk1, and all major VEGF-A isoforms, most prominently VEGF-A¹⁶⁴ and VEGF-A¹²⁰ (VEGF-A¹⁶⁵ and VEGF-A¹²¹ in human) (Figure 1C). VEGF-A treatment of ARPE-19 cells induced phosphorylation of VEGFR2 and its downstream target AKT, which could be blocked by a specific VEGFR2 kinase inhibitor (Figure S1C), demonstrating that VEGF-A can elicit VEGFR2-dependent VEGF-A pathway activation in RPE cells.

VEGF-A pathway activation can lead to RPE barrier breakdown of RPE monolayers in vitro (Ablonczy et al., 2011). To test whether increased VEGF-A levels in VEGF-A^{hyper} mice are associated with RPE barrier disruption, choroidal flatmounts from these mice were stained for β -catenin and zonula occludens-1 (ZO-1). In RPE cells of young VEGF-A^{hyper} mice and in healthy control mice, immunolabeling for β -catenin and ZO-1 shows a membrane-bound localization, as β -catenin is part of the adherens junctions and ZO-1 is part of the tight junctions, both comprising the RPE barrier. In adult VEGF-A^{hyper} mice focal RPE cytoskeletal abnormalities were observed with loss of the typical RPE honeycomb cell morphology, and these changes were associated with loss of membrane-bound ZO-1 and β -catenin and their increased cytoplasmic and nuclear accumulation, providing a morphologic correlate to RPE barrier breakdown (Figures 1D-E). These changes were observed in all

VEGF-A^{hyper} mice examined, while they were not seen in any control littermate mice (>200 mutant and control mice were examined between the ages 4 weeks to 24 months of age).

While young VEGF-A^{hyper} mice showed multiple small foci of RPE barrier breakdown and morphological abnormalities of the RPE (Figure 1G), aged mice (>7 months old) showed large confluent areas of these defects, mostly in the central part of the posterior eye (Figures 1H-I). Thus, a chronic increase of VEGF-A levels is sufficient to cause an age-dependent progressive RPE barrier breakdown in vivo. Furthermore, VEGF-A treatment of human RPE monolayers resulted in a rapid breakdown of barrier function in FITC-dextran flux assays (Figure 1F), suggesting that the observed RPE barrier breakdown in VEGF-A^{hyper} mice is a direct consequence of increased VEGF-A levels. To provide further evidence for a direct role of VEGF-A for RPE barrier breakdown in vivo, mice were generated that become heterozygous for VEGF-A postnatally specifically in patches of the RPE and carry the VEGF-A^{hyper} allele (VMD2-Cre^{+/-}-VEGF-A^{fl/WT}-VEGF-A^{hyper} mice). In these mice, foci of RPE barrier breakdown were observed primarily at areas of the RPE with absence of Cre expression (and thus increased VEGF-A levels), and not in Cre-positive RPE patches (with normalized VEGF-A levels) (Figure 1L).

Increased VEGF-A levels are associated with cardinal features of nonexudative AMD

Eyes from VEGF-A^{hyper} mice and control mice were examined up to 24 months of age, revealing an age-dependent progressive RPE atrophy and degenerative changes with loss of RPE pigment granules in mutant mice (Figures 2D, S2C, and S2G). While young mutant mice have a normal morphological appearance of most of the RPE and retina (Figure 2B), older mice showed progressive degeneration of the RPE, with some RPE cells undergoing cell death with positive staining for cleaved caspase 3 (Asp175) (Figure 2J). The RPE defects were associated with severe progressive age-dependent degeneration of the photoreceptors, with shortening of the photoreceptor outer and inner segments and a significant attenuation of the photoreceptor nuclear cell layer (ONL) (Figures 2D-E, S2G, and S2H). Apoptotic nuclei of photoreceptors were also observed and rhodopsin levels were significantly reduced in retinas of aged VEGF-A^{hyper} mice (Figures 2F, S2G and S3G), reflecting photoreceptor degeneration. Electron microscopy revealed massive age-dependent electron-dense sub-RPE deposit formation (Figures 2H, S2B, and S2E), strongly resembling basal laminal deposits in AMD. Droplet-like electron-lucent spaces within these deposits (Figures 2H, S2C and S2D) indicate lipid accumulation removed during fixation, as has been reported in basal laminal deposits in human AMD (Curcio et al., 2005b), further supported by Oil Red O-positive sub-RPE accumulations (Figure 2I). Furthermore, “wide-spaced collagen”-like material could be seen in these sub-RPE deposits (Figure S2B), a typical finding in human AMD. These deposits were not observed in young VEGF-A^{hyper} mice, while sub-RPE deposits increased progressively with age. Vacuolar degeneration of RPE cells (Figures S2E and S2F), also found in human eyes with early AMD (Anderson et al., 2002), was an early sign of RPE damage and could already be seen focally in the eyes of young VEGF-A^{hyper} mice, before the onset of photoreceptor loss (Figures 5A and S3C). In addition, round phalloidin-negative autofluorescent droplet-like sub-RPE deposits accumulated with progressive age particularly at sites where RPE cells had lost their normal honeycomb pattern morphology (Figures S2I-J, and Figures 4D-G; these deposits were also negative for F4/80 as seen in Figure S3E).

Thus, a chronic increase of VEGF-A levels leads to early degenerative changes in the RPE and progressive basal laminal sub-RPE deposit formation with subsequent degeneration of photoreceptors. Choroidal vessels maintained endothelial fenestrations and perfusion experiments with fluorescein-labeled lectins did not show a significant abnormality in choroidal perfusion, suggesting that the RPE degeneration is not a consequence of a choroidal vascular perfusion defect (Figure 3A).

Progressive CNV as in neovascular AMD in VEGF-A^{hyper} mice

Disruption of the RPE barrier would be expected to lead to degeneration of photoreceptors and accumulation of a subretinal inflammatory cell infiltrate. Indeed, at sites of RPE barrier breakdown increased photoreceptor apoptosis was seen in VEGF-A^{hyper} mice (Figure S3G), as well as a subretinal myeloid cell inflammatory infiltrate (Figures S3E and S3H).

It has been hypothesized that RPE barrier breakdown and a proangiogenic myeloid cell inflammatory infiltrate promotes CNV in neovascular AMD, although direct evidence for this hypothesis is missing. Eyes from VEGF-A^{hyper} mice showed focal early vacuolar degeneration of RPE cells already at ~4-6 weeks of age, while overlying photoreceptors were intact (Figures 5A, S3C).

The first observed changes in the retina overlying RPE defects showed migration of retinal Muller glia cells towards sites of RPE degeneration (Figure 5A), which dramatically accumulated with progressive age at sites of RPE defects and replaced photoreceptors (Figures 5B). Subsequently, progressive formation of CNV lesions was observed at sites of increased RPE degeneration, starting in young mice and progressing to large confluent multifocal CNV lesions in aged mice (Figures 3A-D, S3I-K). The proliferating new vessels in CNV lesions were perfused through the choroidal vasculature (Figures 3A-B). RPE cells overlying CNV lesions showed increased RPE barrier breakdown with cytoplasmic β -catenin accumulation (Figures 3F and S3K-L) and degenerative atrophic changes (Figure S3A-B), linking RPE-barrier breakdown with CNV formation.

CNV lesions in VEGF-A^{hyper} mice showed striking resemblance to neovascular AMD lesions in humans with the formation of neovascular membranes and loss of the overlying photoreceptors (Figures 3C-E). While the photoreceptor layer was attenuated throughout the retina with increasing age associated with RPE degenerative changes, a cardinal feature of nonexudative AMD, a complete loss of the photoreceptor layer was limited to the retina overlying CNV lesions (Figures 3D and 5B), as is typically seen in neovascular AMD. At sites of CNV lesion formation, retinal Muller glia cells completely replaced photoreceptors with progressive age (Figure 5B). Thus, VEGF-A^{hyper} mice develop cardinal features of both nonexudative and neovascular AMD with progressive age.

NLRP3 inflammasome activation in mice with increased VEGF-A levels

To identify molecular mechanisms that promote the AMD-like pathologies in aged VEGF-A^{hyper} mice, RPE cells were isolated from eyes of aged VEGF-A^{hyper} mice and control littermate mice for gene expression profiling experiments. Among the highly upregulated genes in the RPE of VEGF-A^{hyper} mice were the inflammasome component NLRP3, IL-1 and the complement cascade component C1q (Table S1). It has recently been reported that the NLRP3 inflammasome is activated in AMD, but the significance of NLRP3 inflammasome activation for the pathogenesis of AMD is not known and has not been validated in an animal model that reflects the human disease process (Kaneko et al., 2011; Tarallo et al., 2012; Doyle et al., 2012). The complement pathway component C1q, found in drusen in AMD, was shown to activate the NLRP3 inflammasome in peripheral blood mononuclear cells in vitro, but whether NLRP3 inflammasome activation in macrophages plays a pathogenic role for AMD has not been shown (Doyle et al., 2012). Fatty acids have also been shown to be able to activate the NLRP3 inflammasome, and these lipids are also found in drusen and basal laminar deposits in AMD (Curcio et al., 2005a; Duewell et al., 2010; Wen et al., 2011). Similarly, the basal laminar sub-RPE deposits in aged VEGF-A^{hyper} mice showed evidence for lipid deposition by electron microscopy and Oil red O staining (which binds triglycerides, esterified cholesterols and fatty acids) (Figure 2I), which may promote inflammasome activation in the RPE of these mice.

Immunostaining showed strong NLRP3 expression in RPE cells predominantly within CNV lesions in VEGF-A^{hyper} mice (Figures 3G, S4A), linking increased RPE barrier breakdown and RPE degeneration with NLRP3 inflammasome activation and subsequent neovascularization. In addition, strong accumulation of C1q was observed in a perivascular pattern in CNV lesions (Figures 3H-I), consistent with the gene expression profiling results and its reported role as an NLRP3 inflammasome activator.

In ARPE-19 cells oxidative stress can activate the NLRP3 inflammasome (Kauppinen et al., 2012). Notably, VEGF has been shown to induce oxidative stress in endothelial cells, while challenging RPE cells in vitro with oxidants increased VEGF-A levels (Klettner and Roider, 2009; Monaghan-Benson and Burrige, 2009) ENREF 6. Consistent with these observations, VEGF-A treatment resulted in a rapid and significant increase of oxidative stress (determined by measuring superoxide reaction with dihydroethidium) in ARPE-19 cells (Figure 3K), and staining for acrolein (a marker for oxidative damage-induced lipid peroxidation) (Dorrell et al., 2009) was increased focally in RPE cells of aged VEGF-A^{hyper} mice (Figure 3J), suggesting that a chronic increase of VEGF-A results in increased oxidative damage in RPE cells.

Mice with deficiency of the anti-oxidant enzyme SOD1, resulting in increased superoxide levels, develop with progressive age RPE barrier breakdown and some AMD-like pathologies, albeit much more delayed and less striking than VEGF-A^{hyper} mice (Imamura et al., 2006). As oxidative stress results in an increase in VEGF-A levels in RPE cells in vitro, and SOD1 null mice phenocopy to some degree VEGF-A^{hyper} mice, it is possible that the observed AMD-like pathologies in SOD1 null mice may be mediated in part by increased VEGF-A levels. Indeed, VEGF-A serum levels in young SOD1 null mice, prior to the manifestation of AMD-like pathologies, were increased compared to control littermate mice (Figure 3L), further suggesting that increased VEGF-A levels are central to the development of AMD-like pathologies. Oxidative stress induced by SOD1 knockdown in ARPE-19 cells (as well as in a lens epithelial cell line) resulted in increased IL-1 levels in the cell culture supernatant (Figure 3M), demonstrating a contributory role of oxidative stress to inflammasome activation in RPE cells as well.

Thus, degenerative RPE changes following VEGF-A induced RPE barrier breakdown in VEGF-A^{hyper} mice are associated with increased sub-RPE lipid- and complement C1q-deposits and increased oxidative damage, all factors promoting inflammasome activation. To test whether in VEGF-A^{hyper} mice NLRP3 inflammasome activation occurs, the protein levels of the active caspase-1 subunits p10 and p20 were examined, which are derived from caspase-1 precursor through autocatalytic cleavage when the inflammasome is activated. Western blotting confirmed activation of the inflammasome with increased p10 and p20 active subunits in RPE/choroid tissues of aged VEGF-A^{hyper} mice, while control littermate mice showed no inflammasome activation (Figure 4A). Furthermore, immunostaining showed co-expression of NLRP3 and p10 focally in the RPE/choroid of aged VEGF-A^{hyper} mice, consistent with NLRP3 inflammasome activation (Figures 4B, and S4B-C).

Choroidal flatmounts from aged VEGF-A^{hyper} mice showed that increased NLRP3 expression was limited to degenerative RPE cells that had lost their typical honeycomb appearance, while no NLRP3 expression was seen in normal appearing adjacent RPE cells or macrophages (Figures 4C and S4D). Notably, NLRP3 expression and degenerative changes of RPE cells were often seen in association with a large number of round extracellular autofluorescent deposits that were phalloidin-negative (average diameter: $25.6\mu\text{m} \pm 6.8\mu\text{m}$; average area of $574.8\mu\text{m}^2 \pm 190.8\mu\text{m}^2$) (Figures 4D-G).

Targeting the NLRP3 inflammasome inhibits AMD-like pathologies in VEGF-A^{hyper} mice

To test whether NLRP3 inflammasome activation in VEGF-A^{hyper} mice contributes to VEGF-A induced AMD pathologies, NLRP3 or the inflammasome effector cytokines IL-1 and IL-18 were targeted genetically in VEGF-A^{hyper} mice. NLRP3, IL-1 receptor type 1 and IL-18 null mice showed no AMD-like pathologies. Notably, targeting NLRP3, IL-1 receptor type 1 (abolishing IL-1 signaling) or IL-18 in VEGF-A^{hyper} mice did not prevent the observed chorioretinal pathologies and double-mutant mice showed RPE-barrier breakdown, RPE degeneration and multifocal CNV lesions with macrophage infiltration as seen in VEGF-A^{hyper} mice (Figures 4H, and S4E-G). However, deficiency of NLRP3 or IL-1 receptor type 1 in VEGF-A^{hyper} mice reduced the number of CNV lesions that formed in 6 week-old mice, while deficiency in IL-18 resulted in a significantly increased number of CNV lesions compared to double-mutant VEGF-A^{hyper} mice lacking IL1R1 or NLRP3 (Figure 4I). VEGF-A protein levels in the RPE/choroid, retina or serum were not increased in IL-18 null mice compared to NLRP3 or IL1R1 null mice, suggesting that IL-18 deficiency promotes CNV lesion formation through VEGF-A-independent mechanisms (data not shown). Thus, NLRP3 inflammasome activation and the resulting increase in active IL-1, which acts as a potent proangiogenic factor, promote VEGF-A induced AMD-pathologies, such as RPE barrier breakdown and CNV lesion formation.

Macrophages activate proangiogenic retinal glia cells to promote CNV

To determine which cell types are critical for promoting CNV, the spatiotemporal cellular events that lead to CNV lesion formation in VEGF-A^{hyper} mice were analyzed. Retinal Muller cell accumulation and increased glial fibrillary acid protein (GFAP) expression occur in human AMD retinas, but the significance of these Muller cells for AMD pathogenesis is not known (Wu et al., 2003). Eyes of VEGF-A^{hyper} mice showed a progressive increase of GFAP expression in retinal cells overlying evolving CNV lesions (Figures 5C-F). In young mutant mice at sites of accumulation of a myeloid cell infiltrate between the RPE and the retina, GFAP expression in cells of the overlying retina was increased and Muller cells migrated towards the RPE prior to neovessel formation (Figure 5C). Strong GFAP staining and retinal Muller cell accumulation was observed subsequently in evolved CNV lesions (Figures 5D-E). Increased N-cadherin expression was also observed in Muller cells at sites of evolving CNV lesions, a marker for proliferating glia cells (Figure S5h). These findings suggest that RPE barrier breakdown and macrophage infiltration into the space between the retina and the RPE occur first, and that these macrophages subsequently activate retinal Muller glia cells to promote CNV.

While infiltrating macrophages in VEGF-A^{hyper} mice do not stain for VEGF-A (-gal-), RPE cells in CNV lesions strongly expressed VEGF-A (Figures 5I and S3E). Overlying retinal glia cells that infiltrated CNV lesions strongly expressed VEGF-A as well (Figures 5H-I). Furthermore, these cells showed high expression of the proangiogenic cytokine IL-1 and of IL-18 and co-labeling for GFAP confirmed that these cells were retinal Muller glia cells (Figures 5G-K, and S5A-D). Choroidal flatmounts, in which the retina was removed, showed glia Muller cells adhering to the RPE and infiltrating CNV lesions and that these cells were the main source of IL-1 in CNV lesions (Figure S5E). Glia cells infiltrated degenerative RPE cells particularly at sites with high density of autofluorescent sub-RPE deposits (Figures S5G and S5I).

The observations in CNV formation in VEGF-A^{hyper} mice suggest that RPE defects and barrier breakdown are followed by a macrophage infiltrate into the space between the retina and the RPE that activates retinal Muller glia cells, which promote CNV through secretion of proangiogenic factors including VEGF-A and IL-1. If this sequence of events is required for neovascularization, ablation of the myeloid cell infiltrate should result in reduced glia

cell activation and inhibition of subsequent neovascularization. This hypothesis was tested in a laser-injury model of CNV, in which disruption of the RPE barrier is achieved through a laser that targets the pigmented RPE cells and leads to subsequent CNV lesions through proliferation of blood vessels at the site of laser injury. While this acute injury model is limited in the assessment of the role of chronic changes for AMD pathogenesis, it allows the characterization of acute spatiotemporal events during neovascularization in the choroid (He and Marneros, 2013). Similar as in CNV lesion formation in VEGF-A^{hyper} mice, time-course experiments showed that in the laser-injury model of CNV macrophages infiltrate the site of laser injury early, followed by the formation of a NG2⁺SMA⁺ myofibroblastic scaffold into which Muller glial cells infiltrate, before neovascularization occurs (Figures 6A-G). Like in CNV lesions in VEGF-A^{hyper} mice, VEGF-A expression could not be detected in macrophages in laser-induced CNV lesions, but VEGF-A expression was seen in RPE cells as well as glia cells overlying CNV lesions, which also expressed IL-1 (Figures S6A-D). Low-level NLRP3 expression was observed only in few RPE cells in laser lesions, and not in lesional macrophages (Figure S6E-F). NLRP3 protein levels in lysates from pooled choroids of wild-type mice 3 days after laser injury were much lower and almost undetectable when compared to choroid lysates from age-matched unlasered VEGF-A^{hyper} mice (Figure S6G), suggesting that VEGF-A^{hyper} mice are better suited to investigate the role of the NLRP3 inflammasome for CNV than the laser-injury wounding model.

Macrophage populations after wound injury undergo an M2-like polarization with expression of the prototypic M2-macrophage marker Arg1. Consistent with the CNV laser-injury model representing an acute wound healing model of neovascularization, immunolabeling for Arg1 and F4/80 confirmed that most macrophages that accumulate at sites of laser-injury are Arg1⁺F4/80⁺ M2-like macrophages, while non-lesional choroidal F4/80⁺ cells were Arg1⁻ (Figure S6H). In human AMD eyes a mixed macrophage infiltrate has been reported, with both M1 and M2 macrophage populations occurring (Cao et al., 2011). Similarly, only a subset of macrophages in spontaneous CNV lesions in aged VEGF-A^{hyper} mice was Arg1⁺ (Figure S6I), reflecting the mixed macrophage populations in human AMD eyes, which is consistent with a chronic progressive eye pathology.

Next, mutant mice were generated in which temporal ablation of macrophages can be induced through injection of diphtheria toxin (Lysozyme M Cre-iDTR homozygous mice). Temporal ablation selectively of macrophages in these mice inhibited the formation of the SMA⁺NG2⁺ myofibroblastic scaffold and glia cell accumulation in laser lesions, and reduced subsequent neovascularization significantly (Figures 6H-O). Thus, macrophages promote glia cell activation with expression of VEGF-A and IL-1 and subsequent choroidal neovascularization.

Discussion

The findings in aged VEGF-A^{hyper} mice reveal that a chronic increase in VEGF-A levels is sufficient to cause age-dependent cardinal features of both nonexudative AMD and neovascular AMD, providing a unifying pathomechanism for advanced AMD. These features are likely to be a consequence of both direct as well as indirect effects of increased VEGF-A signaling, such as through the induction of downstream pathways and cellular changes. The findings are consistent with the clinical observation that neovascular AMD can often co-occur with nonexudative AMD, and highlights the notion that AMD can occur along a spectrum with the manifestations of features of both neovascular and nonexudative forms (Sunnness et al., 1999).

AMD has been proposed to be a multifactorial disease and various risk factors for AMD have been identified, including smoking, advanced age, chronic light exposure and genetic

risk factors (Friedman et al., 2004; Klein et al., 2004; van Leeuwen et al., 2003). The observations of cardinal features of AMD in aged VEGF-A^{hyper} mice that only differ from their control littermates by increased VEGF-A levels, suggest that in AMD multiple risk factors may converge to cause mainly RPE hypoxia and oxidative damage, which stimulate increased VEGF-A expression in RPE cells (Klettner and Roeder, 2009). Thus, although advanced AMD may result from multi-factorial insults to the RPE in humans, aged VEGF-A^{hyper} mice serve as a mouse model for AMD due to a single genetic alteration that leads to increased VEGF-A levels, demonstrating a central role of increased VEGF-A signaling in AMD pathogenesis.

The observation in VEGF-A^{hyper} mice that early RPE degenerative changes are seen prior to photoreceptor loss, provides *in vivo* evidence that the RPE is at the center of the disease process in AMD and that retinal degeneration occurs as a consequence of an impaired RPE function.

Increased VEGF-A levels are shown here to lead to RPE barrier breakdown and progressive degenerative changes in the RPE, which are associated with accumulation of lipid-rich basal laminar sub-RPE deposits and complement C1q, and an increase in oxidative damage, similarly as in human eyes with AMD. These RPE abnormalities are linked to NLRP3 inflammasome activation, focal RPE cell death, and CNV lesion formation. Targeting NLRP3 or IL-1 β -signaling in these mice reduced RPE barrier breakdown and CNV lesion formation, demonstrating that the NLRP3 inflammasome contributes to VEGF-A induced AMD-like pathologies. IL-18 deficiency had an opposite effect on CNV lesion formation, suggesting an anti-angiogenic effect of IL-18 (Doyle et al., 2012). While NLRP3 deficiency increased the size of laser injury-induced neovascular lesions in an acute wound-healing model in the eye (Doyle et al., 2012), an inhibition of CNV lesion number was observed here in VEGF-A^{hyper} mice that lack NLRP3. These differences are not surprising, as in the acute laser-injury model neovascularization occurs in the setting of healthy RPE cells that show little or no NLRP3 expression and neovascularization occurs within 4 days after injury, while CNV lesions in VEGF-A^{hyper} mice develop over a prolonged period of time and occur in the setting of RPE-barrier breakdown and VEGF-A associated accumulation of C1q and oxidative damage, with strong expression of NLRP3 and inflammasome activation, similar as in human AMD.

It is further shown here that RPE barrier breakdown leads to accumulation of macrophages into the space between the RPE and the retina, with subsequent activation of retinal Muller glia cells that strongly express the proangiogenic factors IL-1 β and VEGF-A to promote CNV. These findings are consistent with observations that showed human neovascular AMD lesions to contain a large number of IL-1 β expressing cells and RPE cells to express VEGF-A (Oh et al., 1999).

In summary, aged VEGF-A^{hyper} mice serve as an important new mouse model for both forms of AMD, and reveal a central role of increased VEGF-A and NLRP3 inflammasome activation for RPE degeneration and AMD pathogenesis. Preventative strategies to reduce RPE hypoxia or therapeutically target increased VEGF-A-signaling in RPE cells in combination with blocking IL-1 β or the NLRP3 inflammasome could therefore inhibit both forms of AMD.

Experimental Procedures

Animals

The generation of VEGF-A^{hyper} mice and VEGF-A^{hypo} mice was previously reported (Miquerol et al., 1999) (Damert et al., 2002). VEGF-A^{hyper} mice were crossed with IL-18^{-/-},

IL1R1^{-/-} or NLRP3^{-/-} mice to obtain mice that are heterozygous for the VEGF-A^{hyper} allele and homozygous null for IL18, IL1R1 or NLRP3 (JAX laboratories)(Takeda et al., 1998; Glaccum et al., 1997; Brydges et al., 2009).

Immunolabeling

Eyes were fixed in 4% paraformaldehyde. For choroidal flatmounts eyes were permeabilized in 0.5% Triton X and subsequently blocked with serum in which the secondary antibodies were raised. A full description of antibodies used is provided in the Extended Experimental Procedures. Staining for β -galactosidase activity was performed as described previously (Marneros et al., 2005).

Western blotting

Eye tissues from VEGF-A^{hyper} mice and control littermate mice of different ages were used for Western blotting experiments. Freshly dissected posterior eye poles were lysed in NP40 lysis buffer with 1mM PMSF and protease inhibit cocktail using the Qiagen TissueLyserII. After centrifugation the supernatant was used for Western blotting. A full description of antibodies used is provided in Extended Experimental Procedures.

Experimental CNV model

Eyes of age- and gender-matched mice were exposed to laser photocoagulation for induction of experimental CNV after eyes were dilated with 1% tropicamide and mice were anesthetized with 75 mg/kg ketamine and 7.5 mg/kg xylazine. Laser photocoagulation was performed using a 532nm laser (Zeiss Visulas 532S). Lesions were induced using a power of 200mW, a spot size of 50 μ m, and a duration of 100ms as previously described (He and Marneros, 2013).

Supplementary Material

Refer to Web version on PubMed Central for supplementary material.

Acknowledgments

I would like to thank Drs. Andras Nagy, Lucile Miquelol and Annette Damert for providing VEGF-A^{hyper} and VEGF-A^{hypo} mice, and Dr Napoleone Ferrara for providing VEGF-A^{fl/fl} mice. This work was supported by a grant to A.G.M. from the NEI R01-EY019297. A.G.M. designed the project, performed experiments, analyzed the data and wrote the manuscript.

References

- Ablonczy Z, Dahrouj M, Tang PH, Liu Y, Sambamurti K, Marmorstein AD, Crosson CE. Human retinal pigment epithelium cells as functional models for the RPE in vivo. *Invest Ophthalmol Vis Sci.* 2011; 52:8614–8620. [PubMed: 21960553]
- Anderson DH, Mullins RF, Hageman GS, Johnson LV. A role for local inflammation in the formation of drusen in the aging eye. *American journal of ophthalmology.* 2002; 134:411–431. [PubMed: 12208254]
- Bird AC, Bressler NM, Bressler SB, Chisholm IH, Coscas G, Davis MD, de Jong PT, Klaver CC, Klein BE, Klein R, et al. An international classification and grading system for age-related maculopathy and age-related macular degeneration. The International ARM Epidemiological Study Group. *Surv Ophthalmol.* 1995; 39:367–374. [PubMed: 7604360]
- Brydges SD, Mueller JL, McGeough MD, Pena CA, Misaghi A, Gandhi C, Putnam CD, Boyle DL, Firestein GS, Horner AA, et al. Inflammasome-mediated disease animal models reveal roles for innate but not adaptive immunity. *Immunity.* 2009; 30:875–887. [PubMed: 19501000]

- Cao X, Shen D, Patel MM, Tuo J, Johnson TM, Olsen TW, Chan CC. Macrophage polarization in the maculae of age-related macular degeneration: a pilot study. *Pathol Int.* 2011; 61:528–535. [PubMed: 21884302]
- Cervi D, Shaked Y, Haeri M, Usenko T, Lee CR, Haigh JJ, Nagy A, Kerbel RS, Yefenof E, Ben-David Y. Enhanced natural-killer cell and erythropoietic activities in VEGF-A-overexpressing mice delay F-MuLV-induced erythroleukemia. *Blood.* 2007; 109:2139–2146. [PubMed: 17053052]
- Curcio CA, Presley JB, Malek G, Medeiros NE, Avery DV, Kruth HS. Esterified and unesterified cholesterol in drusen and basal deposits of eyes with age-related maculopathy. *Exp Eye Res.* 2005a; 81:731–741. [PubMed: 16005869]
- Curcio CA, Presley JB, Millican CL, Medeiros NE. Basal deposits and drusen in eyes with age-related maculopathy: evidence for solid lipid particles. *Experimental eye research.* 2005b; 80:761–775. [PubMed: 15939032]
- Damert A, Miquerol L, Gertsenstein M, Risau W, Nagy A. Insufficient VEGFA activity in yolk sac endoderm compromises haematopoietic and endothelial differentiation. *Development.* 2002; 129:1881–1892. [PubMed: 11934854]
- Dorrell MI, Aguilar E, Jacobson R, Yanes O, Gariano R, Heckenlively J, Banin E, Ramirez GA, Gasmi M, Bird A, et al. Antioxidant or neurotrophic factor treatment preserves function in a mouse model of neovascularization-associated oxidative stress. *J Clin Invest.* 2009; 119:611–623. [PubMed: 19188685]
- Doyle SL, Campbell M, Ozaki E, Salomon RG, Mori A, Kenna PF, Farrar GJ, Kiang AS, Humphries MM, Lavelle EC, et al. NLRP3 has a protective role in age-related macular degeneration through the induction of IL-18 by drusen components. *Nat Med.* 2012; 18:791–798. [PubMed: 22484808]
- Duewell P, Kono H, Rayner KJ, Sirois CM, Vladimer G, Bauernfeind FG, Abela GS, Franchi L, Nunez G, Schnurr M, et al. NLRP3 inflammasomes are required for atherogenesis and activated by cholesterol crystals. *Nature.* 2010; 464:1357–1361. [PubMed: 20428172]
- Friedman DS, O'Colmain BJ, Munoz B, Tomany SC, McCarty C, de Jong PT, Nemesure B, Mitchell P, Kempen J. Prevalence of age-related macular degeneration in the United States. *Arch Ophthalmol.* 2004; 122:564–572. [PubMed: 15078675]
- Fritsche LG, Chen W, Schu M, Yaspan BL, Yu Y, Thorleifsson G, Zack DJ, Arakawa S, Cipriani V, Ripke S, et al. Seven new loci associated with age-related macular degeneration. *Nat Genet.* 2013; 45:433–439. [PubMed: 23455636]
- Funk M, Karl D, Georgopoulos M, Benesch T, Sacu S, Polak K, Zlabinger GJ, Schmidt-Erfurth U. Neovascular age-related macular degeneration: intraocular cytokines and growth factors and the influence of therapy with ranibizumab. *Ophthalmology.* 2009; 116:2393–2399. [PubMed: 19815292]
- Glaccum MB, Stocking KL, Charrier K, Smith JL, Willis CR, Maliszewski C, Livingston DJ, Peschon JJ, Morrissey PJ. Phenotypic and functional characterization of mice that lack the type I receptor for IL-1. *Journal of immunology.* 1997; 159:3364–3371.
- He L, Marneros AG. Macrophages Are Essential for the Early Wound Healing Response and the Formation of a Fibrovascular Scar. *The American journal of pathology.* 2013
- Imamura Y, Noda S, Hashizume K, Shinoda K, Yamaguchi M, Uchiyama S, Shimizu T, Mizushima Y, Shirasawa T, Tsubota K. Drusen, choroidal neovascularization, and retinal pigment epithelium dysfunction in SOD1-deficient mice: a model of age-related macular degeneration. *Proc Natl Acad Sci U S A.* 2006; 103:11282–11287. [PubMed: 16844785]
- Jafarifar F, Yao P, Eswarappa SM, Fox PL. Repression of VEGFA by CA-rich element-binding microRNAs is modulated by hnRNP L. *The EMBO journal.* 2011; 30:1324–1334. [PubMed: 21343907]
- Kaneko H, Dridi S, Tarallo V, Gelfand BD, Fowler BJ, Cho WG, Kleinman ME, Ponicsan SL, Hauswirth WW, Chiodo VA, et al. DICER1 deficit induces Alu RNA toxicity in age-related macular degeneration. *Nature.* 2011; 471:325–330. [PubMed: 21297615]
- Kauppinen A, Niskanen H, Suuronen T, Kinnunen K, Salminen A, Kaarniranta K. Oxidative stress activates NLRP3 inflammasomes in ARPE-19 cells-Implications for age-related macular degeneration (AMD). *Immunol Lett.* 2012

- Klein R, Peto T, Bird A, Vannewkirk MR. The epidemiology of age-related macular degeneration. *Am J Ophthalmol.* 2004; 137:486–495. [PubMed: 15013873]
- Klettner A, Roeder J. Constitutive and oxidative-stress-induced expression of VEGF in the RPE are differently regulated by different Mitogen-activated protein kinases. *Graefes Arch Clin Exp Ophthalmol.* 2009; 247:1487–1492. [PubMed: 19603178]
- Kliffen M, van der Schaft TL, Mooy CM, de Jong PT. Morphologic changes in age-related maculopathy. *Microsc Res Tech.* 1997; 36:106–122. [PubMed: 9015257]
- Latz E, Xiao TS, Stutz A. Activation and regulation of the inflammasomes. *Nat Rev Immunol.* 2013; 13:397–411. [PubMed: 23702978]
- Marneros AG, Fan J, Yokoyama Y, Gerber HP, Ferrara N, Crouch RK, Olsen BR. Vascular endothelial growth factor expression in the retinal pigment epithelium is essential for choriocapillaris development and visual function. *Am J Pathol.* 2005; 167:1451–1459. [PubMed: 16251428]
- Martin DF, Maguire MG, Ying GS, Grunwald JE, Fine SL, Jaffe GJ. Ranibizumab and bevacizumab for neovascular age-related macular degeneration. *N Engl J Med.* 2011; 364:1897–1908. [PubMed: 21526923]
- Miquerol L, Gertsenstein M, Harpal K, Rossant J, Nagy A. Multiple developmental roles of VEGF suggested by a LacZ-tagged allele. *Dev Biol.* 1999; 212:307–322. [PubMed: 10433823]
- Monaghan-Benson E, Burridge K. The regulation of vascular endothelial growth factor-induced microvascular permeability requires Rac and reactive oxygen species. *The Journal of biological chemistry.* 2009; 284:25602–25611. [PubMed: 19633358]
- Oh H, Takagi H, Takagi C, Suzuma K, Otani A, Ishida K, Matsumura M, Ogura Y, Honda Y. The potential angiogenic role of macrophages in the formation of choroidal neovascular membranes. *Invest Ophthalmol Vis Sci.* 1999; 40:1891–1898. [PubMed: 10440240]
- Sunness JS, Gonzalez-Baron J, Bressler NM, Hawkins B, Applegate CA. The development of choroidal neovascularization in eyes with the geographic atrophy form of age-related macular degeneration. *Ophthalmology.* 1999; 106:910–919. [PubMed: 10328389]
- Takeda K, Tsutsui H, Yoshimoto T, Adachi O, Yoshida N, Kishimoto T, Okamura H, Nakanishi K, Akira S. Defective NK cell activity and Th1 response in IL-18-deficient mice. *Immunity.* 1998; 8:383–390. [PubMed: 9529155]
- Tarallo V, Hirano Y, Gelfand BD, Dridi S, Kerur N, Kim Y, Cho WG, Kaneko H, Fowler BJ, Bogdanovich S, et al. DICER1 loss and Alu RNA induce age-related macular degeneration via the NLRP3 inflammasome and MyD88. *Cell.* 2012; 149:847–859. [PubMed: 22541070]
- Tseng WA, Thein T, Kinnunen K, Lashkari K, Gregory MS, D'Amore PA, Ksander BR. NLRP3 inflammasome activation in retinal pigment epithelial cells by lysosomal destabilization: implications for age-related macular degeneration. *Investigative ophthalmology & visual science.* 2013; 54:110–120. [PubMed: 23221073]
- van Leeuwen R, Klaver CC, Vingerling JR, Hofman A, de Jong PT. Epidemiology of age-related maculopathy: a review. *Eur J Epidemiol.* 2003; 18:845–854. [PubMed: 14561043]
- Wen H, Gris D, Lei Y, Jha S, Zhang L, Huang MT, Brickey WJ, Ting JP. Fatty acid-induced NLRP3-ASC inflammasome activation interferes with insulin signaling. *Nat Immunol.* 2011; 12:408–415. [PubMed: 21478880]
- Wen H, Ting JP, O'Neill LA. A role for the NLRP3 inflammasome in metabolic diseases--did Warburg miss inflammation? *Nature immunology.* 2012; 13:352–357. [PubMed: 22430788]
- Wilkie AL, Jordan SA, Jackson IJ. Neural crest progenitors of the melanocyte lineage: coat colour patterns revisited. *Development.* 2002; 129:3349–3357. [PubMed: 12091305]
- Wu KH, Madigan MC, Billson FA, Penfold PL. Differential expression of GFAP in early v late AMD: a quantitative analysis. *Br J Ophthalmol.* 2003; 87:1159–1166. [PubMed: 12928288]
- Yu Y, Bhangale TR, Fagerness J, Ripke S, Thorleifsson G, Tan PL, Souied EH, Richardson AJ, Merriam JE, Buitendijk GH, et al. Common variants near FRK/COL10A1 and VEGFA are associated with advanced age-related macular degeneration. *Hum Mol Genet.* 2011; 20:3699–3709. [PubMed: 21665990]

Highlights

1. An increase in VEGF-A is sufficient to cause cardinal features of both “wet” and “dry” AMD
2. Increased VEGF-A results in defects of the RPE that lead to activation of the NLRP3 inflammasome
3. Targeting the NLRP3 inflammasome inhibits VEGF-A induced AMD, while IL-18 inhibition promotes AMD
4. Macrophages promote “wet” AMD through activation of proangiogenic retinal glia cells

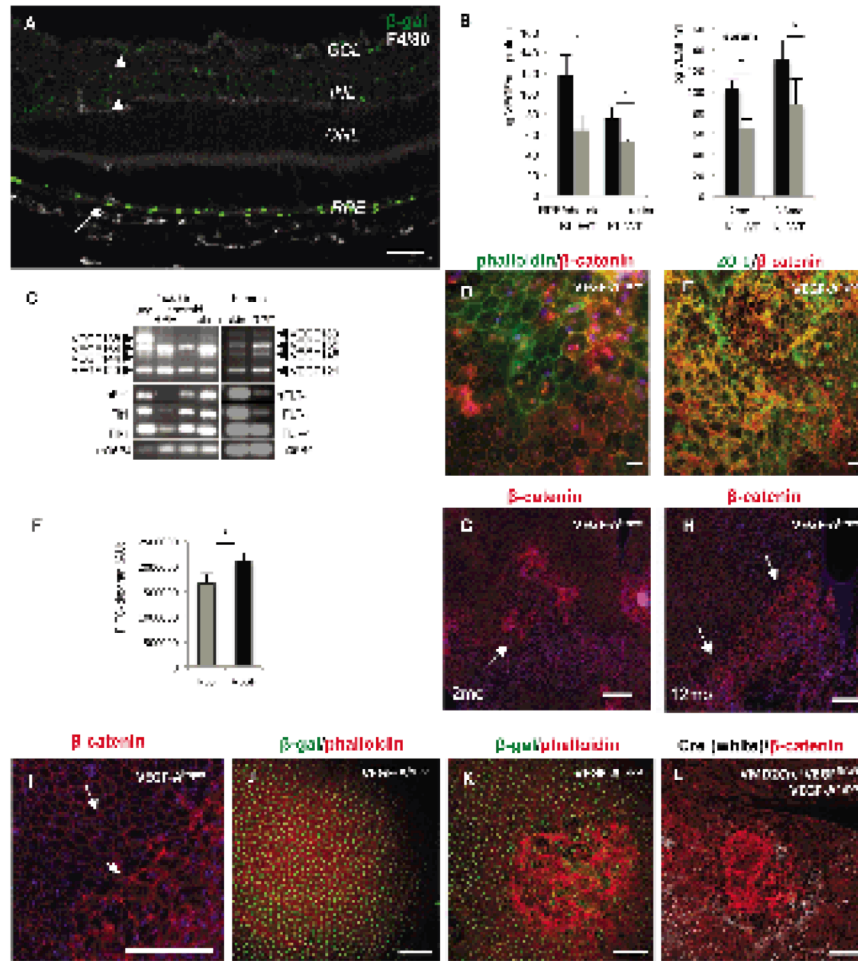


Figure 1. Increased VEGF-A levels result in a progressive RPE barrier breakdown

a. The RPE is the main cell type of VEGF-A expression in the adult eye. Immunolabeling of an adult posterior eye of a VEGF-A^{hyper} mouse (15 months old) for β -galactosidase reflects cellular expression of VEGF-A (green). Strong VEGF-A expression is observed in RPE cells (arrow), whereas low-level VEGF-A expression is seen in retinal cells of the ganglion cell layer (GCL) and inner nuclear layer (INL) (arrowheads), but not the photoreceptor layer (outer nuclear layer; ONL). Scale bar 50 μ m.

b. VEGF-A ELISA of RPE/choroid and retinal tissue in adult VEGF-A^{hyper} mice (KI) and control littermate (WT) mice (n=7/group) shows a significant increase of VEGF-A levels in the RPE/choroid tissues in VEGF-A^{hyper} mice. Serum levels of VEGF-A are elevated in mutant mice independently of age as well (n=3/group). *P-value <0.05.

c. Mouse and human RPE cells express the VEGF-A receptors Flt1 and Flk1 and all major VEGF-A isoforms, particularly VEGF-A¹⁶⁴ and VEGF-A¹²¹ (VEGF-A¹⁶⁵ and VEGF-A¹²¹ in human).

d. Focal RPE barrier breakdown is observed in VEGF-A^{hyper} mice with cytoplasmic and nuclear accumulation of β -catenin. Co-labeling with Alexa488-conjugated phalloidin (green) shows that in normal RPE cells phalloidin and β -catenin (red) labeling is strongest along cell membranes, while in RPE cells with RPE barrier breakdown β -catenin labeling along the cell membranes is attenuated and increased in the nuclei or cytoplasm. 7 months old VEGF-A^{hyper} mouse. Scale bar 20 μ m.

- e. Co-labeling of cell junction proteins β -catenin (red) and ZO-1 (green) shows loss of membrane-bound ZO-1 and β -catenin with nuclear accumulation. 7 months old VEGF-A^{hyper} mouse. Scale bar 50 μ m.
- f. FITC-dextran flux assays with RPE cells demonstrate that VEGF-A¹⁶⁵ treatment induces barrier breakdown and increased transepithelial flux of 10kDa FITC-dextran. (n=3), *P-value <0.05. y-axis indicates fluorescence units (AU).
- g-h. Choroidal flatmount staining of eyes from VEGF-A^{hyper} mice with β -catenin (red) shows that RPE-barrier breakdown is observed in small foci (arrow) in young VEGF-A^{hyper} eyes (2 months old, (g)), but that these areas expand and become confluent and affect most of the posterior eye (arrows) with progressive age of the mice (12 months old, (h)). Scale bars 200 μ m.
- i. Magnification of area from Figure 1H that delineates normal appearing RPE with its honeycomb pattern from lesional abnormal appearing RPE cells. Scale bar 200 μ m.
- j. Adult VEGF-A^{hypo} mice, hypomorphic for VEGF-A, express β -galactosidase (green) from the endogenous VEGF-A gene locus, but show normal RPE cells. Scale bar 100 μ m.
- k. In contrast, adult VEGF-A^{hyper} mice, with increased VEGF-A levels, show the same expression of β -galactosidase (green) from the endogenous VEGF-A gene locus as VEGF-A^{hypo} mice, but show multifocal RPE barrier breakdown. Scale bar 100 μ m.
- l. Mice that express VMD2-Cre specifically in RPE cells (white nuclear staining for Cre) that are heterozygous for VEGF-A^{fl/fl} and carry the VEGF-A^{hyper} allele; in these mice Cre⁺ RPE cells are expected to have lower levels of VEGF-A than Cre⁻ RPE cells. RPE barrier breakdown occurs predominantly within Cre⁻ RPE-patches (therefore expressing higher levels of VEGF-A). Scale bar 100 μ m. See also Figure S1.

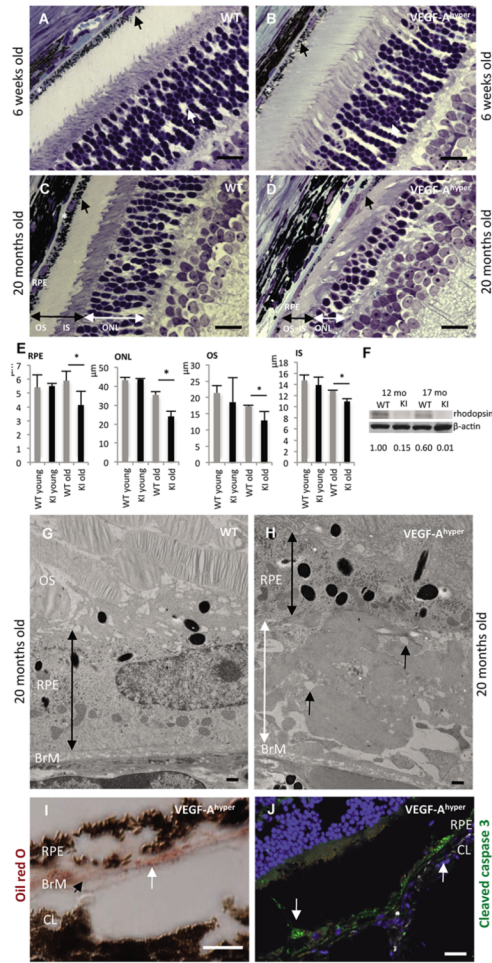


Figure 2. Progressive age-dependent degeneration of the RPE and photoreceptors in mice with increased VEGF-A levels

a.-d. While the retina and choroid/RPE appear unremarkable in young adult VEGF-A^{hyper} mice (6 weeks old, b), with progressive age a severe RPE atrophy is noticed with loss of pigment granules, thinning of RPE cells and massive sub-RPE deposit accumulation (black arrow, d). The photoreceptor nuclear layer (ONL) is severely attenuated (white double arrow, d) compared to age-matched littermate control retinas (c). In addition, photoreceptor inner and outer segments (black double arrow) are significantly shortened (d). Scale bar 20µm. * indicates Bruch's membrane.

e. Quantification of RPE and photoreceptor length reveals significantly thinned RPE and attenuated photoreceptor outer (OS), inner (IS) segments and ONL in aged mutant mice (20 months of age). *P-value <0.05.

f. Photoreceptor degeneration is reflected in reduced rhodopsin protein levels in posterior eyes of aged VEGF-A^{hyper} mice (KI, 12 and 17 months old) compared to control littermate mice (WT). Normalized densitometric values are indicated.

g.-h. Electron microscopy demonstrates massive accumulation of basal laminar sub-RPE deposits in aged (20 months old, h) VEGF-A^{hyper} mice compared to age-matched control littermate mice (g). The RPE is thinned in VEGF-A^{hyper} mice (black double arrow) and sub-RPE deposits (white double arrow) consist of electron-dense deposits resembling basal laminar deposits and electron-lucent spaces indicate lipid-like material that was removed during fixation (black arrows). BrM: Bruch's membrane. OS: photoreceptor outer segments. Scale bars 500nm.

i. Oil red O staining in an aged VEGF- A^{hyper} mouse shows accumulation of lipid droplets in sub-RPE deposits (white arrow). Black arrowhead points to Bruch's membrane (BrM). CL: Choroidal layer. Scale bar 10 μm .

j. RPE cell degeneration in aged VEGF- A^{hyper} mice (15 months old) with RPE cells focally undergoing cell death, demonstrated by cleaved caspase 3 (Asp175) immunostaining (white arrows). CL: choroid layer Scale bar 50 μm . See also Figure S2.

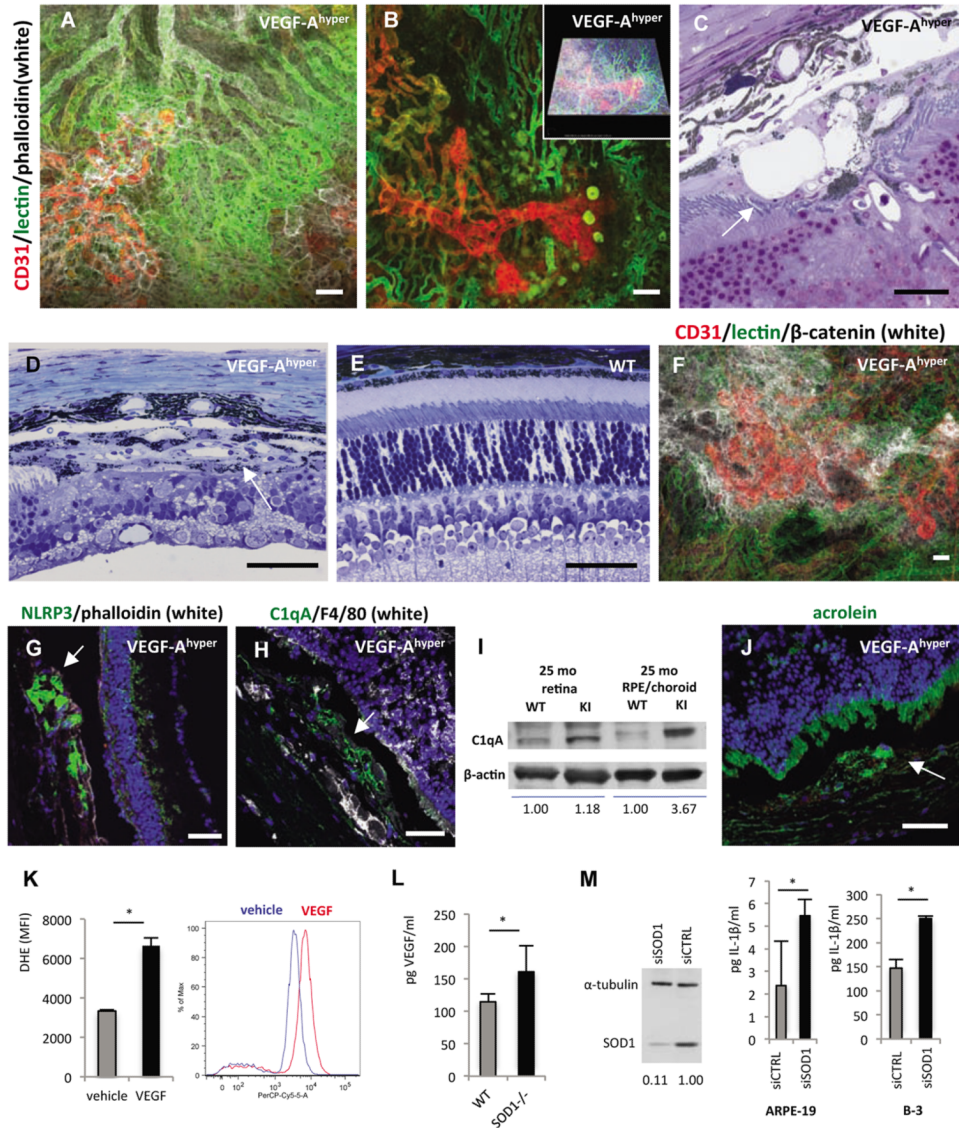


Figure 3. Choroidal neovascularization and NLRP3 expression in aged VEGF-A^{hyper} mice
 a.-b. Perfusion experiments in aged white VEGF-A^{hyper} mice with fluorescein-conjugated tomato lectin and subsequent wholemount staining for CD31 and phalloidin shows that proliferating neovessels (CD31, red) originate from the underlying perfused choroidal vasculature (green) and extend into the sub-RPE space. Autofluorescent round deposits can be seen at sites of CNV lesions. Scale bars 50µm. Inset in b. represents modeled z-stack of lesion.
 c. Representative section of CNV lesion in aged VEGF-A^{hyper} mice shows massive subretinal neovascularization (arrow). Scale bar 20µm.
 d. Representative image of a fully formed CNV lesion in a 7 months old VEGF-A^{hyper} mouse that resembles a neovascular membrane in neovascular AMD (arrow). Neovascularization and fibrosis have completely replaced the photoreceptor layer at the site of CNV formation. Scale bar 50µm.
 e. In age-matched control littermate mice such lesions were not seen. Scale bar 50µm.
 f. Co-localization of RPE barrier breakdown with CNV lesions. Choroidal flatmount of a 24 months old white VEGF-A^{hyper} mouse in which choroidal perfusion is assessed by

intracardiac administration of a fluorescein-conjugated tomato lectin (green). Subsequent whole-mount staining for CD31 (red) highlights proliferating neovessels from underlying perfused choroidal vessels (green), and labeling for β -catenin (white) shows RPE barrier breakdown at sites of neovascularization with cytoplasmic accumulation of β -catenin. Scale bar 50 μ m.

g. Strongly increased NLRP3 expression in RPE cells in CNV lesions (arrows) with attenuation or loss of the overlying photoreceptor layer. 15 months old VEGF-A^{hyper} mice. Scale bars 50 μ m.

h. Perivascular accumulation of C1qA within CNV lesions (arrow). 15 months old VEGF-A^{hyper} mice. Scale bar 50 μ m.

i. Western blotting demonstrates accumulation of C1qA in choroid/RPE tissues of aged VEGF-A^{hyper} mice, while control littermate mice showed no accumulation of C1qA. Choroid/RPE or retinal tissues represent pools from three 25 months old VEGF-A^{hyper} mice or control mice. Normalized relative densitometric values are indicated.

j. Acrolein, a marker for ROS-induced lipid peroxidation, is increased focally in abnormal RPE cells in aged VEGF-A^{hyper} mice (green, arrow) (15 months old). DAPI nuclear staining; photoreceptor outer segments show autofluorescence (green). Scale bar 50 μ m.

k. VEGF-A¹⁶⁵ treatment of ARPE-19 cells loaded with 10 μ M dihydroethidium (DHE) induces increased oxidative stress (superoxide indicator), measured by FACS (PerCP-Cy5-5 channel). Y-axis shows mean fluorescence intensity (MFI) of triplicate experiments (n=3/group). A representative histogram demonstrates the shift of fluorescence induced by VEGF-A¹⁶⁵, representing increased superoxide species. *P-value <0.05.

l. VEGF-A serum levels are increased in young (7 weeks old) SOD1^{-/-} mice, compared to age- and gender-matched control littermate mice (n=5). *P-value <0.05.

m. SOD1 is efficiently depleted using SOD1-targeted siRNA, demonstrated by Western blotting of ARPE-19 cell lysate. Cell culture supernatant of cells, primed with 4ng/ml IL-1 β , shows that SOD1 knockdown increases levels of the inflammasome effector cytokine IL-1 β in both ARPE-19 cells and the B-3 lens epithelial cells. N=4/group. *P-value <0.05. See also Figure S3.

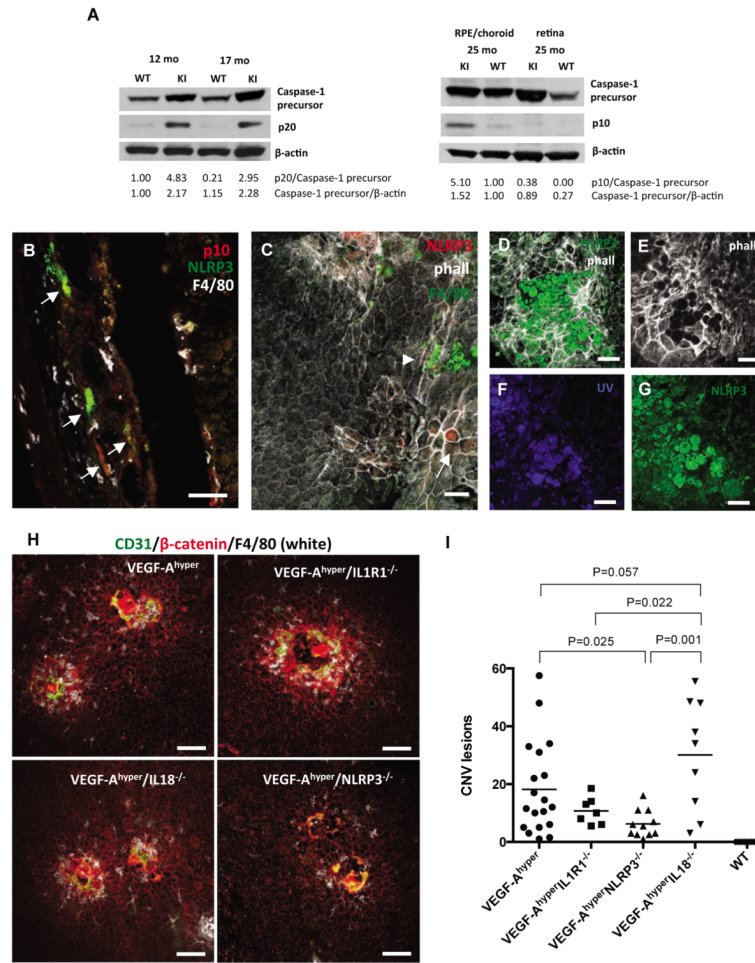


Figure 4. Blockade of the NLRP3 inflammasome reduces CNV lesions in VEGF-A^{hyper} mice
 a. Left: Western blotting of posterior eye lysates from 12 and 17 months old VEGF-A^{hyper} mice (KI) and control littermate mice (WT) shows activation of the inflammasome with strong upregulation of the caspase-1 active subunit p20 in mutant mice. Right: Pools of RPE/choroid or retinal tissue from three 25 months old VEGF-A^{hyper} mice (KI) and control littermate mice (WT) show strong upregulation of the p10 caspase-1 active subunit in the RPE/choroid, but not in the retina, demonstrating inflammasome activation in RPE/choroid tissues of VEGF-A^{hyper} mice. Normalized densitometric values are indicated.
 b. NLRP3 (green, arrows) is strongly expressed in RPE cells in VEGF-A^{hyper} mice (15 months old). Macrophages are stained with F4/80 (white). Co-labeling for the activated p10 subunit of caspase-1 (red) with NLRP3 (green) shows inflammasome activation. Scale bar 50 μ m.
 c. NLRP3 immunostaining of choroidal flatmounts with expression of NLRP3 in RPE cells that show abnormal cellular morphology (phalloidin, white; arrow), while normal appearing RPE cells with typical honeycomb cytoarchitecture do not express NLRP3 (red). (13 months old). No NLRP3 expression is seen in F4/80⁺ macrophages (green, arrowhead). Scale bar 50 μ m.
 d.-g. Round autofluorescent extracellular deposits accumulate at sites of RPE degeneration in aged VEGF-A^{hyper} mice (21 months old). These round deposits are phalloidin-negative (e), and show autofluorescence with UV-light (f), or the green light channel (g), which also shows increased NLRP3 immunostaining at sites of these deposits. Scale bar 50 μ m.

h. RPE barrier breakdown (β -catenin, red), macrophage infiltration (F4/80, white) and CNV lesion formation (CD31, green) occurs in VEGF-A^{hyper} mice, despite genetic inactivation of IL-1R1, NLRP3 or IL-18. Representative images of choroidal flatmounts from 6 week old mice. Scale bars 100 μ m.

i. Quantitative analysis of CNV lesion numbers per age-matched mutant mice (6 weeks old) in choroidal flatmounts (average CNV lesion numbers/mouse of choroidal flatmounts stained for β -catenin and CD31). No CNV lesions were seen in WT control mice. P-values were determined with a two-tailed Student's t-test. N>7 mice/group. See also Figure S4.

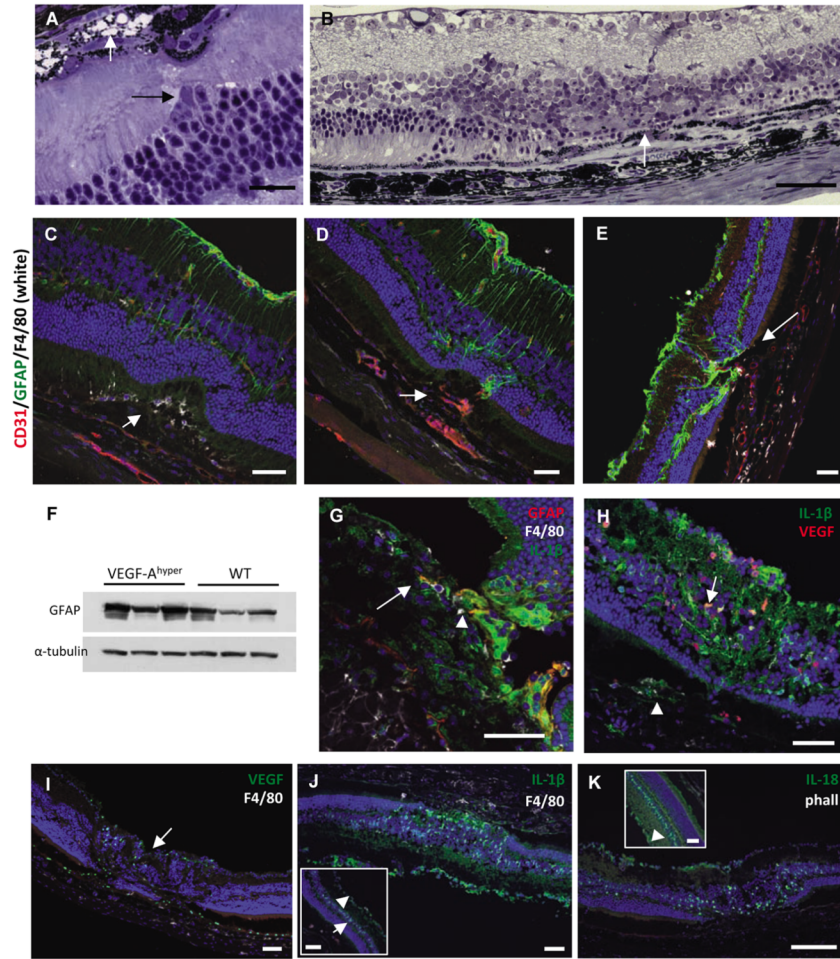


Figure 5. Glia cell activation in CNV lesions in VEGF-A^{hyper} mice

- a. In young VEGF-A^{hyper} mice (6 weeks old) early RPE degeneration is seen only focally with some RPE cells undergoing vacuolar degeneration (intracellular vacuoles with remaining pigment granules; black arrow). At this stage retinal changes are limited, but migration of retinal Muller gliocells (white arrow) towards sites of RPE degeneration can already be observed. Scale bar 20 μ m.
- b. In aged VEGF-A^{hyper} mice the photoreceptor layer adjacent to CNV lesions is present, but attenuated. Complete loss of photoreceptors is seen in retina overlying CNV lesions with an accumulation of retinal Muller gliocells (arrow). Scale bar 50 μ m. 21 months old VEGF-A^{hyper} mouse.
- c. At sites of early evolving CNV lesions subretinal macrophages (F4/80⁺, white; arrow) are seen prior to neovessel formation. Limited to the overlying retina GFAP expression (green) increases, indicating glia cell activation and proliferation, while adjacent retina appears unchanged. Scale bar 50 μ m. 4 months old VEGF-A^{hyper} mouse.
- d. In early CNV lesions with subretinal neovascularization (CD31, red; arrow) GFAP⁺ glia cells have increased and have infiltrated early CNV lesions (green). Scale bar 50 μ m. 4 months old VEGF-A^{hyper} mouse.
- e. In aged VEGF-A^{hyper} mice with large CNV lesions, massive GFAP expression and glia cell infiltration into sites of CNV lesion formation is seen (arrow). Scale bar 50 μ m. 15 months old VEGF-A^{hyper} mouse.
- f. Retinal GFAP is increased in aged VEGF-A^{hyper} mice compared to littermate control mice. 16 months old mice.

g. Co-immunolabeling for GFAP (red), IL-1 β (green) and F4/80 (white), shows that high IL-1 β expression is seen in infiltrating retinal glia cells (arrowhead), while lower levels are observed in RPE cells and only in few macrophages in CNV lesions (arrow). No IL-1 β is detected in most choroidal macrophages. Scale bar 50 μ m. 15 months old VEGF-A^{hyper} mouse.

h. Retinal glia cells co-express both VEGF-A and IL-1 β in the retina overlying CNV lesions where the photoreceptor layer is severely attenuated (arrow). Labeling for IL-1 β and VEGF-A is also seen in RPE cells (arrowhead) in CNV lesions. Scale bar 50 μ m. 15 months old VEGF-A^{hyper} mouse.

i. Increased VEGF-A expression (green) is seen in retinal glia cells overlying CNV lesions (arrow). Scale bar 50 μ m. 15 months old VEGF-A^{hyper} mouse.

j. While IL-1 β is expressed in glia cells overlying CNV lesions that have replaced the ONL, adjacent normal appearing retina (inset) shows only weak IL-1 β expression in the INL (arrow) and GCL (arrowhead). Scale bars 50 μ m. 15 months old VEGF-A^{hyper} mouse.

k. Infiltrating retinal glia cells show strong expression of IL-18 overlying CNV lesions. Scale bar 50 μ m. 15 months old VEGF-A^{hyper} mouse. See also Figure S5.

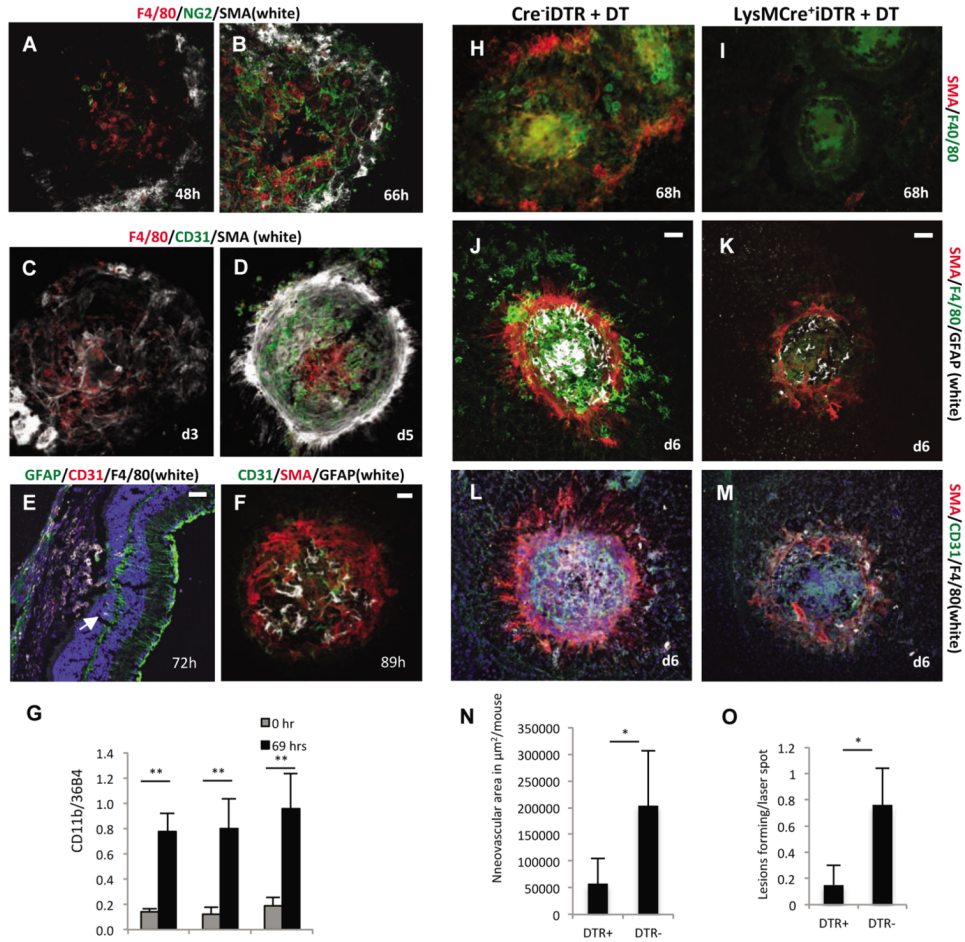


Figure 6. Macrophages are required for retinal glia cell activation and subsequent neovascularization

a.-b. A fibroblast-like scaffold forms after macrophage (red) infiltration that is positive for NG2 (green) and SMA (white). 10× magnification.

c. The fibroblast-like scaffold forms prior to infiltration of the laser-injury site with endothelial cells, as the first CD31⁺ endothelial cells are seen at about 68 hours after injury, when the NG2⁺SMA⁺scaffold has already formed. 10× magnification.

d. Neovascularization occurs after macrophage infiltration and after the formation of the SMA⁺scaffold and fully formed CNV lesions are seen at day 5 (CD31, green). The SMA⁺ scaffold covers the neovascular lesions, resembling a scar after wound injury. 10× magnification. Control mice.

e. GFAP⁺ retinal glia cells (arrow) infiltrate the laser injury site already by 72 hours, before endothelial cells have populated the site. Scale bar 50μm.

f. At day 4 after laser injury new blood vessels form at the site of laser injury after GFAP⁺ cells have already infiltrated the SMA⁺ scaffold. Scale bar 50μm. a.-f. Control mice.

g. Semiquantitative RT-PCR of choroidal tissue lysates shows an increase of macrophages at 69 hours after laser injury (CD68 levels normalized to 36B4 house-keeping gene), consistent with the immunolabeling results. Macrophage accumulation occurs independently of IL10 or STAT6 signaling. N=5/group. **P-value <0.01.

h.-i. Homozygous LysMCre⁺iDTR mice were used for DT injections to temporally and selectively ablate myeloid cells in laser-injury experiments and compared to Cre⁻iDTR mice. DT treatment potently diminished F4/80⁺ macrophage infiltration into the laser-injury site,

assessed here at 68 hours after injury. Ablation of macrophages also inhibited the SMA⁺ scaffold formation (i).

j.-k. Ablation of macrophages inhibited GFAP⁺ glia cell activation (white) and infiltration into the site of laser injury.

l.-m. Inhibition of macrophage infiltration and glia cell activation resulted in a significant inhibition of neovascularization. Only few CD31⁺ vessels (green) were seen at laser-injury sites in which macrophage accumulation was reduced, while full neovascular lesions formed in mice with no ablation of macrophages. Scale bars 50μm.

n.-o. Reduced CNV lesion formation was seen in mice with selective ablation of macrophages, with a reduction in the total neovascular area and the rate of CNV lesion formation for each laser injury administered. N=20 mice/group. *P-value <0.05. See also Figure S6.